Starting Performance Improvement of Line-Start Permanent-Magnet Synchronous Motor Using Composite Solid Rotor

Bo Yan[1], Xiuhe Wang[1], and Yubo Yang[1]

[1]School of Electrical Engineering, Shandong University, Jinan, China, sdpmsm@gmail.com

This paper presents a line-start permanent-magnet synchronous motor (LSPMSM) with high starting performance using a composite solid rotor. The rotor is shaped as non-concentricity to alleviate flux waveform distortion and fabricated mainly by solid steel to employ its inherent high starting torque. Moreover, axial slots milled on rotor surface deepen flux penetration into rotor core and a welded squirrel cage made from high-conductive brass increases eddy-current density of the whole rotor, both of which improve the induced torque and hence enable motor to start up and synchronize under large load inertias. A two-dimensional (2D) time-stepping finite element method (FEM), in which the end effect of solid steel and uneven bars distribution are considered by respectively introducing the correction factor and a cage circuit, yields results in good agreement with the corresponding three-dimensional (3D) FEM and provides validation for staring capability of the proposed motor.

Index Terms—**composited solid rotor, LSPMSM, non-concentricity, starting performance.**

I. INTRODUCTION

WITH PROMINENT steady-state advantages of high efficiency, power density and power factor, the line-start permanent-magnet synchronous motors (LSPMSMs) have become competitive substitutes to induction machines in many industrial applications [1]. Squirrel cage of the laminated rotor gives an LSPMSM self-start ability. However, the starting performance is poor. For instances, adding cage resistance to increase induction torque and limit starting currents inversely lowers the synchronization possibility while on the other aspect, reducing size of permanent magnets (PMs) to diminish the braking torque worsens motor steady properties such as the power factor and synchronous torque [2].

To solve these conflicts, this paper presents an LSPMSM with a new composite solid rotor replacing the squirrel-cage one. Appearing as non-concentricity to cut down flux waveform distortion and cogging torque, the rotor is mainly composed by solid steel with its inherent high starting torque. Furtherly, axial slots are milled on rotor surface to yield deeper flux penetration and speed rises in virtue of the reverse relationship between penetration depth and rotor slip [2]. Apart from the slots, a squirrel cage is also welded to the rotor, by which more eddy currents with smaller flowing region but much bigger areal density than those induced in solid steel can be generated and the induction torque is consequently improved. Transient analysis results by two-dimensional (2D) finite element method (FEM), whose calculation accuracy is verified by the relevant three-dimensional (3D) FEM, are implemented to validate the well starting performance of the proposed motor.

II. MOTOR DESIGN

Practically, self-start ability of an LSPMSM comes down to the induction torque T_i which can be expressed as:

$$T_i = \omega_r^{-1} \cdot \sigma^{-1} \cdot \iint_{\substack{induced \\ region}} |J|^2 \cdot dxdy \tag{1}$$

where ω_r stands for angular frequency, σ for equivalent rotor conductivity and J for the eddy-current density.

Under the same rotor slip, the slotted rotor owns much deeper flux penetration than the smooth one and induced region is comparatively enlarged. A squirrel cage effectively increases current density of the whole rotor. According to (1), both axial slots and squirrel cage can be applied to the solid rotor to obtain a larger induction torque.

Considering merits by adding axial slots and squirrel cage, a 6-pole, 50Hz, 10kV, 355kW, three-phase LSPMSM with a new composite solid rotor is designed. Main machine parameters are given in Table I and the 1/3 rotor model is depicted by Fig. 1(a). In this rotor, the PMs are sandwiched by non-concentric solid segments with axial slots and a brass squirrel cage milled on surface. PM slot wedges with large cross-section area also constitute a portion of the cage bars and hence the size and number of other bars can be reduced.

Fig. 1(b) shows the non-concentric rotor outline in which the circle center of rotor surface curve is not aligned with the stator center. The non-concentricity level can be defined by the ratio of the maximum air gap length δ_{max}, to the minimum length δ_{min}. Reasonable ratio selections can effectively lower the flux waveform distortion, reduce cogging torque while deliver little impacts on start-up.
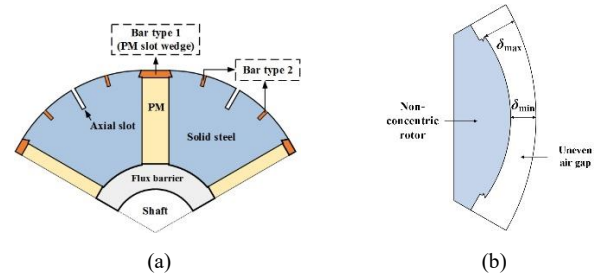

Fig. 1. Prototype of the proposed rotor.

TABLE I
MAIN PARAMETERS OF THE CASE-STUDY MOTOR

Item	Value (unit)	Item	Value (unit)
Stator Outer/ Inner Diameter	740/510 (mm)	The Maximum/ Minimum Air Gap Length $\delta_{max}/\delta_{min}$	12.8/7.5 (mm)
Nominal Inertia (J$_r$)	19.7 kg.m^2	Nominal Load Torque (T$_N$)	3.4 kN.m

III. 2D FEM Calculation

Field equations in the 2D rectangular coordinates can be expressed as:

$$\frac{\partial}{\partial x}\left(v\frac{\partial A_z}{\partial x}\right)+\frac{\partial}{\partial y}\left(v\frac{\partial A_z}{\partial y}\right)=-J_0-J_e-J_m \qquad (2)$$

where A_z is the z component of magnetic vector potential $\mathbf{A}$, J_0 is current density of stator windings, J_e is eddy-current density of rotor and J_m is equivalent magnetizing current density of PMs.

Circuit equations of applied voltage u, induced voltage e and current i for stator windings in star connection are given by [3]:

$$\begin{cases}\dfrac{2}{3}e_a-\dfrac{e_b+e_c}{3}+r_1 i_a+L_1\dfrac{\partial i_a}{\partial t}-u_a=0\\[2mm]\dfrac{2}{3}e_b-\dfrac{e_c+e_a}{3}+r_1 i_b+L_1\dfrac{\partial i_b}{\partial t}-u_b=0\\[2mm]\dfrac{2}{3}e_c-\dfrac{e_a+e_b}{3}+r_1 i_c+L_1\dfrac{\partial i_c}{\partial t}-u_c=0\end{cases} \qquad (3)$$

where subscripts a, b and c represent stator phase quantities, r and L_1 stand for resistance and end-winding leakage inductance of each phase, respectively.

The torque equation is expressed by:

$$T_e=J_r\frac{d\omega_r}{dt}+T_{load} \qquad (4)$$

where T_e and T_{load} are respectively the electromagnetic and load torque, and J_r is the rotational inertia.

Applying the 2D time-stepping FEM [4] can solve (2)-(4) and obtain starting process of the motor. End effect of solid rotor segments can be calculated using correction factor k_{end} [5] which depends on not only the geometry factors but also ω_r. However, due to the varying bar sizes and unevenly distributed end ring fractions, as shown by Fig. 2(a), simply replacing the actual cage impedance by an equivalent one is incorrect. In this paper, an additional cage circuit considering the non-uniform end ring fractions between unequal bars is built in the 2D FEM to represent the actual cage construction. The resistances and inductances of end ring fractions, as illustrated in Fig. 2(b) by circuit elements R_{endi}/L_{endi}, (i=1, 2), are obtained in advance based on design formulas [6] and then the 2D FEM computation executes with the coupled circuit. Calculated results by the 2D method containing k_{end} and the introduced circuit agree well with those of 3D FEM, which is described in the later section.
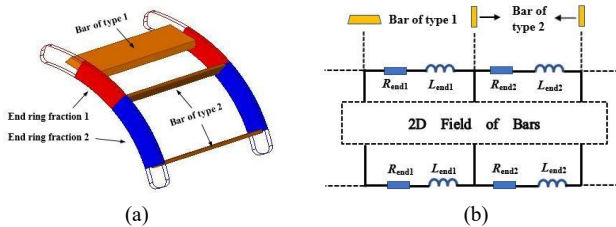

(a) (b)

Fig. 2. Squirrel-cage construction and circuit.

IV. Results Comparison

Firstly, to validate accuracy of the above-mentioned 2D FEM, both of the 2D method and a general 3D FEM are applied to obtain the starting process of the designed motor under nominal load. For the 3D FEM, motor model is constructed as Fig. 3(a).

and Fig.3 (b) shows good agreement between results by the two methods, which proves that the 2D FEM can compute well the end effect of solid steel and end ring fractions sandwiched by various bars in uneven distribution.
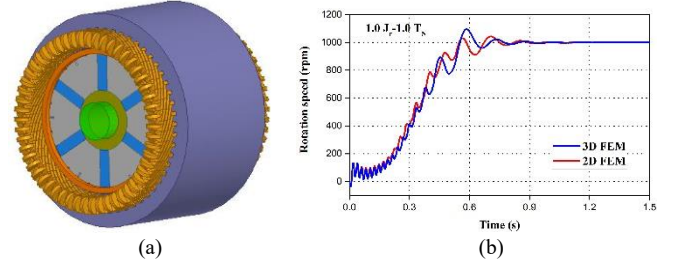

(a) (b)

Fig. 3. Motor model in 3D FEM and results comparison .

Secondly, based on the 2D FEM, starting processes of the designed motor and two other motors (named as M1 and 2) are simultaneously obtained under two load settings, whose load torque is T_N but inertias are much higher than the nominal value, viz. J_r. All these motors have the same stator configuration with each other while the rotors differ. In contrast to the designed one, rotor of M1 is absence of axial slots and squirrel cage is not contained in the rotor of M2.

Fig. 4 shows the start-up comparisons. For the load case of $9\times J_r$, M2 fails in synchronization and the incapability reflects the torque enhancement by adding a squirrel cage. For another load case, in which load torque remains unchanged and the inertia increases to $11\times J_r$, M1 can not reach synchronous speed even a squirrel cage is welded on rotor. The bad performance approves that besides the added cage, slotting on rotor surface is able to furtherly strengthen the driving torque. Conclusion from the two above comparisons can be drawn that the designed motor does hold outstanding synchronization ability due to the added squirrel cage and axial slots on the rotor.
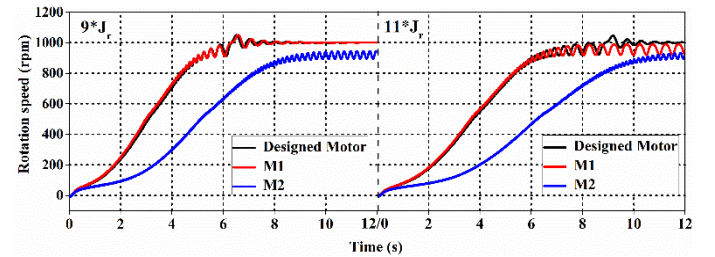

Fig. 4.   Speed-time response comparisons

References

[1] Arash Hassanpour Isfahani and Sadegh Vaez-Zadeh, "Line start permanent magnet synchronous motors: challenges and opportunities," *Elsevier J. Energy*, vol. 34, pp. 1755-1763, Nov. 2009.

[2] Milad Niaz Azari and Mojtaba Mirsalim, "Line-start permanent-magnet motor synchronization capability improvement using slotted solid rotor," *IET Electr. Power Appl.*, vol. 7, pp. 462-469, Jul. 2013.

[3] Kazumi Kurihara and M. Azizur Rahman, "High-efficiency line-start interior permanent-magnet synchronous motors," *IEEE Trans. Ind. Appl.*, vol. 40, pp. 789-796, May/June 2004.

[4] K. Kurihara, G. Wakui and T. Kubota, "Transient performance analysis of permanent magnet synchronous motors," *Trans. Inst. Elect. Eng. Jpn.*, vol. 114-D, pp. 551-560, 1994.

[5] Juha Pyrhonen, Janne Nerg, Panu Kurronen and Uwe Lauber, "High-speed high-output solid-rotor induction-motor technology for gas compression," *IEEE Trans. Ind. Electron.*, vol. 57, pp. 272-280, Jan. 2010.

[6] J. Takeuchi, Design of Electrical Machines. Tokyo, Japan: Ohmsha, 1993.